Special Collection dedicated to Professor Alwyn Davies - Article

Journal of Chemical Research

Journal of Chemical Research
January-February 2022 1–9

DOI: 10.1177/17475198221075301
journals.sagepub.com/home/chl
SAGE

Deposition of metallic silver from versatile amidinate precursors for use in functional materials

Shreya Mrig, Martha A Jennings, Malavika A Bhide, Clare Bakewell and Caroline E Knapp

Abstract

Silver (Ag) amidinate metal organic decomposition precursors of the type: $[Ag_2((ArN)_2C(H))_2]$ (Ar = 2,6-dimethylphenyl (**1**), 2,6-diethylphenyl (**2**) and 2,6-diisopropylphenyl (**3**)) have been used for the first time in the deposition of Ag films on glass with multiple functionalities with potential application in optical/biological sensors or for use in electronic circuitry. Precursors **1–3** were isolated from the reaction of silver acetate with the appropriate ligand in a 1:2 stoichiometry and were characterized by ^{1}H and $^{13}C\{^{1}H\}$ NMR, thermal gravimetric analysis and single crystal X-ray diffraction for **2**. Single-layer depositions at 200 °C on glass substrates via spin coating produced transparent (>90% transmittance) coatings, with well-defined Ag nanoparticles. Multi-layer depositions at 200 °C on glass had a metallic lustre and were found to be conductive ($\rho = 0.916–1.83 \times 10^{-6}\ \Omega$m). All films were strongly adhered and displayed excellent coverage of the substrate. Ag films deposited from **1** to **3** were analysed by grazing incidence X-ray diffraction, X-ray photoelectron spectroscopy, energy-dispersive X-ray analysis and scanning electron microscopy, with optical properties determined by UV-Vis spectroscopy.

Keywords

conductive silver, MOD inks, silver precursors, spin coating, thin films

Date received: 27 October 2021; accepted: 6 January 2022

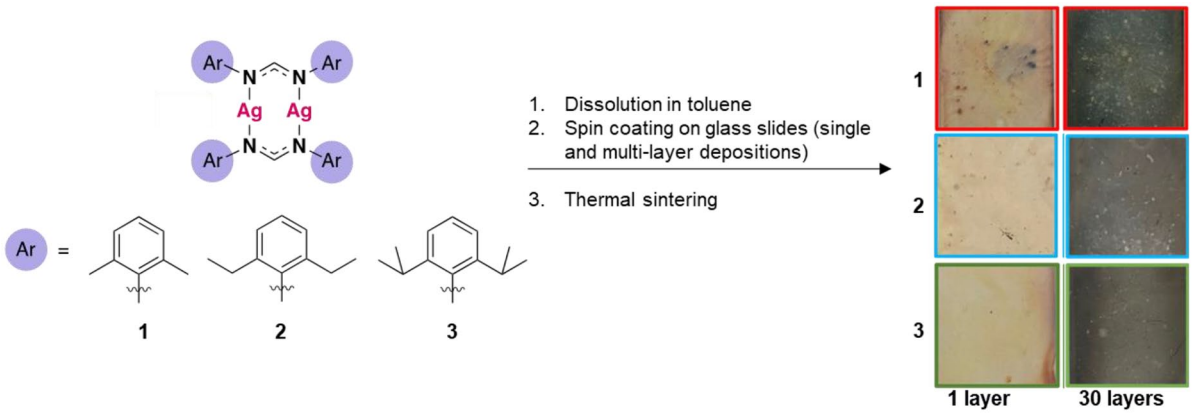

Department of Chemistry, University College London, London, UK

Corresponding authors:
Clare Bakewell, Department of Chemistry, King's College London, 7 Trinity Street, London SE1 1DB, UK.
Email: clare.bakewell@kcl.ac.uk

Caroline E Knapp, Department of Chemistry, University College London, 20 Gordon Street, London WC1H 0AJ, UK.
Email: caroline.knapp@ucl.ac.uk

Introduction

Silver (Ag) is a multi-faceted element which has found uses in various fields.[1] One of the most common uses of Ag is in the electronics industry where it is utilized for its high conductivity to manufacture electrical circuitry for a wide range of electronic devices. Conventional methods of manufacturing conductive Ag circuits, which consume substantial energy and resources, are rapidly being replaced by techniques that allow low-temperature, and less energy intensive manufacture.[2] These new processes rely largely on Ag inks which are deposited onto various substrates and sintered to obtain conductive Ag tracks. Ag nanoparticle (NP) inks are one category of inks that have garnered substantial interest and are becoming a popular choice for deposition of conductive Ag films.[3] Another prevailing use of Ag is in its nanoparticulate form for the manufacture of optical/biological sensors. The localized surface plasmon resonance of the NPs is susceptible to the NP environment;[4] for Ag NPs, a robust surface plasmon resonance is observed, which is not seen in the spectrum of the bulk metal.[5] This property of the nanoparticulate nature of the metal is utilized in the fabrication of these sensors. In addition, the noble nature of the metal offers stability to these deposited Ag NPs which make the metal competent for this use. Both these applications, however, involve the synthesis of Ag NPs with a narrow size distribution which is challenging.[6,7] NP aggregation is a constant hindrance in both these applications which affects the functionality of the final device, while also reducing the shelf life of the inks/complexes. The deposition of NP inks for use in printed electronics also faces issues with printer clogging, high temperature sintering and the need for additives, all of which are detrimental to the final device.[8]

Metal-organic decomposition (MOD) inks are an encouraging alternative to the NP counterparts. MOD inks are composed of MOD precursors in a liquid vehicle that is easy to deposit.[9] The precursors consist of the desired oxidized metal ion bound to suitable ligands. When these precursors are sintered (usually thermally), the compound breaks down to elemental metal (in nanoparticulate form) while the ligands decompose as volatile compounds. Often, the ligands aid the reduction process of the central metal ion to its elemental form.[10] These precursors and subsequent inks are easy to synthesize and store, do not face issues with agglomeration or printer clogging and provide a solution to the issues faced during the synthesis and use of NPs and NP inks.

Ag MOD inks, although not as vastly studied as their NP alternative, have been successfully used to deposit conductive metal. Some of the noticeable work in Ag MOD inks for deposition to conductive metal includes that by Walker and Lewis[11] and Knapp et al.[3] who reported the room temperature deposition of the same ink using plasma sintering to obtain conductive Ag on paper. Other notable works include those by Vaseem et al.[12] and Bhat et al.[13] who synthesized an Ag MOD ink with amines and aminoalcohols as ligands that successfully deposited Ag metal for use in electronics.

Other desired properties of an MOD ink include clean decomposition to target material without residual contaminants,[14] good solubility and long shelf life.[15] Additional pre-requisites for an MOD ink are highlighted in our recent review.[16] All these properties largely depend on the precursor design and ligand selection,[17,18] making these crucial processes for the design of suitable MOD inks.

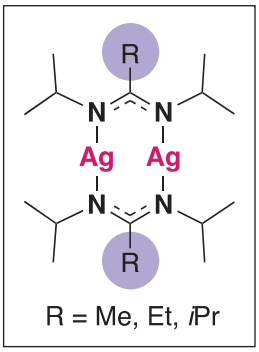

Figure 1. Silver-amidinate complexes synthesized by Whitehorne et al.[20]

An understudied group of ligands for the synthesis of Ag MOD precursors is amidines. A series of Ag-amidinate complexes synthesized for use in catalysis showed impressive thermal properties, with decomposition at ~150 °C, which make them highly promising candidates for MOD precursors.[19] In 2011, Whitehorne et al.[20] were the first to report deposition of Ag using aliphatic amidinates complexed to Ag (Figure 1) via chemical vapour deposition and atomic layer deposition. Thermal gravimetric analysis (TGA) of these compounds showed the reduced metal in the TGA pan with no volatilization occurring. Two potential decomposition pathways were proposed: β-hydrogen elimination and carbodiimide de-insertion.

MOD inks are often criticized for their low metal weight percentage loading due to the presence of the bulky organic ligands. However, they present the opportunity to allow metal deposition for a range of uses. This work reports the synthesis and characterization of three low metal weight percentage loading Ag-amidinate complexes which have then been used to formulate inks to deposit metallic Ag. Given the low weight percentage of Ag in these inks, single-layer depositions have been used to deposit distinct NPs of Ag for use in sensors, while multiple layer depositions were carried out to yield films with a well-connected network of Ag particles, displaying properties similar to that of bulk Ag.

Results and discussion

Precursor synthesis

The amidine ligands were synthesized via modified literature procedures,[21,22] with the 2:1 reaction of 2,6-dimethylphenyl aniline, 2,6-diethylphenyl aniline and 2,6-diisopropylphenyl aniline with triethylorthoformate forming ligands $\mathbf{L^1H}$, $\mathbf{L^2H}$ and $\mathbf{L^3H}$, respectively, in adequate yield (30%–65%). The ^{1}H NMR spectra for all three ligands showed complex patterns of multiplets, suggesting conformationally restricted environments of the phenyl substituents. ^{1}H NMR spectra were recorded at 60 °C, which considerably resolved the multiplets in all cases (Figures S1–S6), indicating only one species is present.

The stoichiometric reaction of $\mathbf{L^1H}$, $\mathbf{L^2H}$ and $\mathbf{L^3H}$ with silver acetate in the presence of triethylamine (NEt_3) in DCM, in the absence of light led to Ag(I) precursors **1–3** of the form $[Ag_2(\mathbf{L}^x)_2]$ (Scheme 1). All compounds were isolated as off white solids in high yield (75%–93%). Complex **2** ($x=2$) is a novel silver(I) amidinate, while **1** ($x=1$) and **3** ($x=3$) have been previously reported.[23]

The ^{1}H NMR spectra of the complexes all show a single ligand environment, indicating that the ligand is conformationally locked upon coordination. Compound **2** has a distinctive triplet at 1.27 ppm (CH_3 groups), and a multiplet at 2.78 ppm corresponding to the diastereotopic methene protons. All compounds also have a distinct set of resonances corresponding to the methine backbone proton due to $^3J_{Ag\text{-}H}$ coupling and retention of the dimeric structure in solution. Ag has an NMR active nucleus with two isotopes (48:52 ratio of ^{109}Ag:^{107}Ag), as such two triplets are observed for the methine backbone proton coupling with the ^{109}Ag-^{109}Ag isotope and ^{107}Ag-^{107}Ag isotope.[24] Finally, the ^{109}Ag-^{107}Ag isotope sees the backbone proton couple first with the ^{109}Ag centre, then with the ^{107}Ag centre resulting in a doublet of doublets (Figure 2).

Crystals of **2** suitable for single crystal X-ray diffraction (XRD) were grown from a methanol/DCM solution which confirmed that, like **1** and **3**, **2** exists as a dimer in the solid state, with the metal centres bridged by the amidinate ligands (Figure 3). **2** crystallized in the triclinic space group $P\bar{1}$. Each Ag(I) centre is coordinated to two amidinate ligands which results in a three-coordinate 'T-shaped' planar environment around the Ag centre. The Ag1-N1, Ag1-Ag1 and Ag1-N2 bond lengths (2.097(2), 2.7432(3) and 2.105(2) Å) and N1-Ag1-Ag1 (83.89(6)°) and N1-Ag1-N2 (168.73(9)°) bond angles were found to be similar to that seen for **1**.

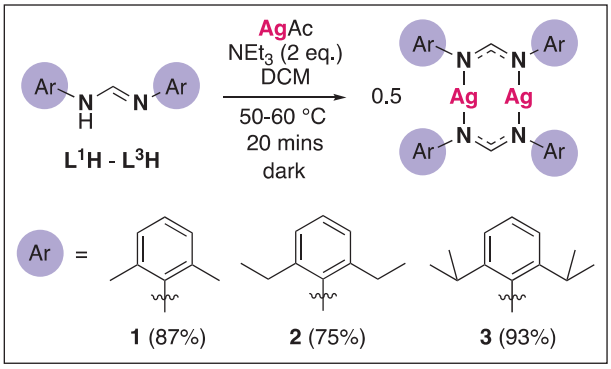

Scheme 1. Synthetic route for the synthesis of Ag(I) amidinate complexes **1–3**.

TGA

To assess the suitability of precursors **1–3** as inks, the decomposition profiles of these compounds were studied by TGA (Figure 4). All three complexes showed clean, one-step decomposition profiles. The onset of decomposition temperature was found to increase as the carbon content of the compounds increased, with **1**, **2** and **3** having onset temperatures of 225, 233 and 250 °C, respectively (Table 1), an observation that might be a result of the increased steric bulk. The compounds showed a mass loss of 51.4%, 59.7% and 66.8% (**1–3**), which is lower than expected for full decomposition to elemental Ag (70.7%, 74.4% and 77.0%). It must be noted that it is possible that some mass was lost to sublimation as this cannot be detected by TGA. This could be a result of incomplete combustion or oxidation of the Ag centre during the heating process. The relatively low-temperature decomposition profiles of the complexes are, however, encouraging.

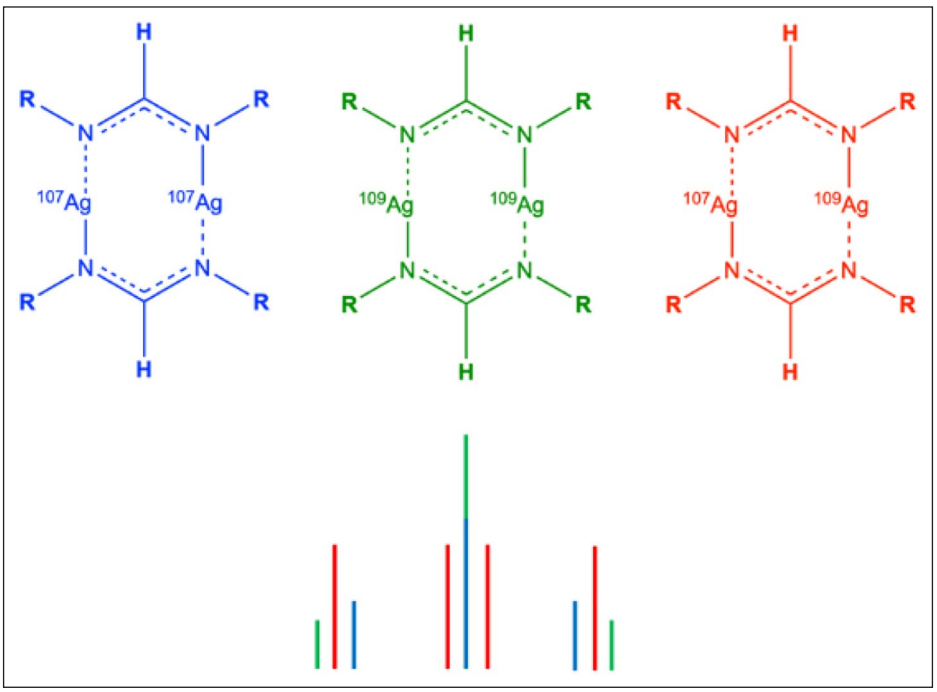

Figure 2. Schematic displaying the overlapping of splitting due to $^3J_{Ag\text{-}H}$ coupling.

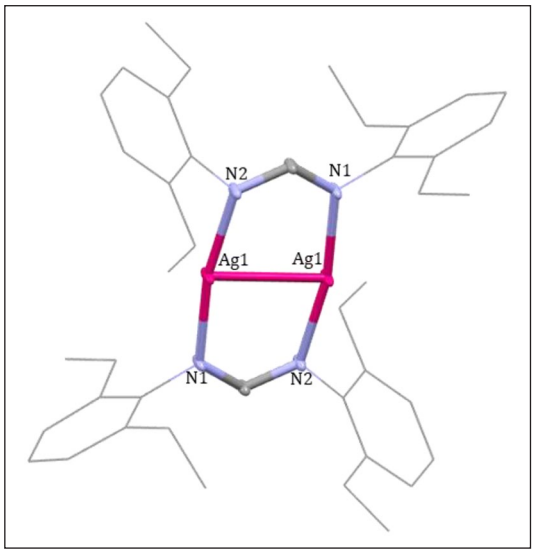

Figure 3. Crystal structure of **2** with thermal ellipsoids drawn at 30% probability. H atoms omitted for clarity. Pink, purple and grey atoms represent Ag, N and C, respectively.

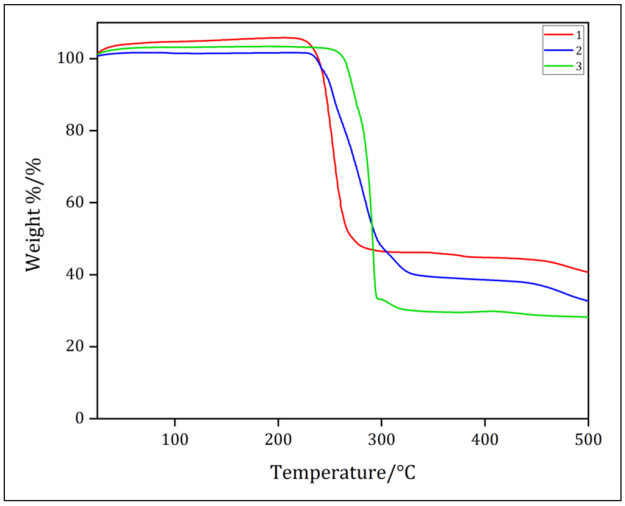

Figure 4. TGA curves and decomposition data for **1–3**.

Table 1. Summary of TGA mass loss (%) and onset temperature (°C).

Precursor	Expected percentage for Ag	Percentage of non-volatile residue (temperature)	Onset temperature
1	29.3	48.6% (279 °C)	225 °C
2	25.6	40.3% (328 °C)	233 °C
3	23.0	33.2% (297 °C)	250 °C

TGA: thermal gravimetric analysis.

Consequently, liquid inks were prepared using solid compounds **1–3**. Following this, the decomposition of these liquid inks was tested by drop casting.

Ink preparation and thin film deposition

To prepare the Ag MOD inks, the solubility of compounds **1–3** was investigated with solvents suitable for thin film deposition. All complexes were found to be soluble in toluene; thus, Ag inks were prepared by dissolving **1–3** in toluene to formulate inks **I1–I3** (0.05 mol dm^{-3}). To test whether these inks convert to elemental Ag, all three inks were initially drop cast onto preheated (200 °C) glass slides and sintered for 15 min. XRD confirmed that all inks converted to elemental Ag, and they were subsequently spin coated onto glass microscope slides at a speed of 1000 r/min for 5 s and sintered at 200 °C for 15 min.

Application of one layer of each ink resulted in transparent deposits, suggesting NP formation rather than aggregated Ag thin film deposition. Scanning electron microscopy (SEM) confirmed the presence of NPs which were not connected, and therefore, the deposits were not conductive (Figure 5). UV-Vis absorption spectra of films deposited from inks **I1**, **I2** and **I3** showed distinctive broad peaks at 461, 459 and 450 nm respectively, attributed to surface plasmon resonance of Ag NPs (Figure 6).[25,26] The single-layer deposits also exhibited high transmittance in the visible region (Figure 7), highlighting the suitability of these deposits in optical/biological sensors.[27] The deposits were too thin to be analysed by XRD, X-ray photoelectron spectroscopy (XPS) and energy-dispersive X-ray analysis (EDX). As our initial drop casting experiments showed that these inks do indeed convert to metallic Ag upon thermal decomposition, we inferred that the deposits produced were extremely thin nanoparticulate coatings of Ag.

Following the single-layer depositions of nanoparticulate Ag, multiple layer depositions were undertaken to fabricate Ag films that could be used in electronics. Inks were deposited in single layers and sintered, with films prepared and analysed between 1 and 30 layers (Due to poor solubility at room temperature, inks **I1** and **I3** had to be reheated to form a homogeneous solution after every four layers of deposition.). The presence of Ag in all films was confirmed by XRD and XPS data. XRD data for all films displayed Braggs peaks at $2\theta = 38.1°$, 44.3° and 64.5° corresponding to the (111), (200) and (220) planes, concurrent with the literature (Figure 8). XPS data were collected through a surface scan at a 300-s etch and showed the presence of metallic Ag, without the presence of any additional peaks. The binding energy was also found to decrease across the series, with films deposited using ink **I3** displaying a lower binding energy than those from inks **I2** and **I1**. The peaks between 373.78 and 374.38 eV are indicative of the Ag $3d_{3/2}$ state[28,29] while the peaks at 367.78–368.38 eV are indicative of the Ag $3d_{5/2}$ transition[30,31] (Figure 9).[3]

Resistance measurements (detailed in the Supplementary Information) showed a decrease in resistance values as the number of layers was increased, with the lowest detectable resistance of 0.1 Ω obtained from 30-layer depositions of **I1**. As the amount of Ag deposited on the substrate increases, the effectiveness of the sintering process improves, allowing for fusion of the Ag particles. This is illustrated in the SEM images of the 30-layered films (Figure 10), which shows a dense network of connected Ag particles. Attempts to spin-coat multiple layers before sintering yielded a non-conductive film that was comparable to the films of one and five layers, thus proving sintering between every layer was required to ensure conductivity occurred.

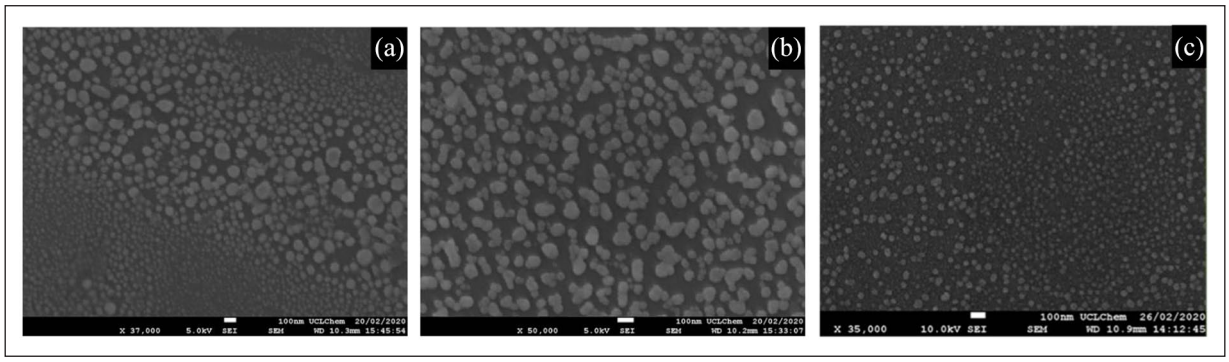

Figure 5. SEM images of single-layer deposits of inks (a) **I1**, (b) **I2** and (c) **I3**.

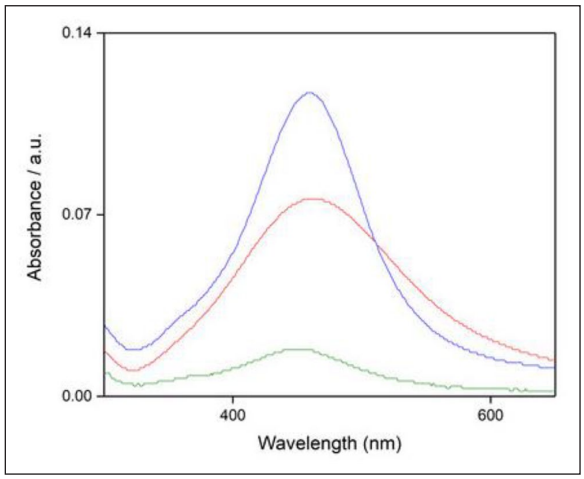

Figure 6. Absorbance spectra of single-layer deposits obtained using inks **I1** (red), **I2** (blue) and **I3** (green).

Side-on SEMs of these films were obtained (Supplementary Information) and were used to calculate the resistivities of the 30-layered films, with resistivity values of 0.916–1.83 × 10^{-6}, 1.575–3.15 × 10^{-6} and 7.25–14.5 × 10^{-6} Ωm from inks **I1**, **I2** and **I3**, respectively (calculated using film thickness data detailed in Supplementary Information), which is comparable to literature values of deposited silver.[32] The lower resistivity of films obtained from **I1** can be attributed to the lower carbon content in the film. Here, the carbon skeleton has decomposed more rapidly, thereby allowing a longer annealing time for the deposited Ag particles. EDX data showed that the Ag content on the surface for films of layers 5 and above was 47%. It also shows that there was no carbon contamination of the films, indicating that during the sintering process, the amidine skeleton completely decomposes, leaving metallic Ag on the surface (The only other observed percentages were Au, which was due to the pre-treating of the sample, Si and O, both of which were due to the glass microscope slide used.). UV-Vis spectra were also obtained for the 30-layered films to compare the optical properties with the single-layered deposits. The absorbance and transmittance of the single- and multi-layered films vary (Figure 7). As the number of layers is increased and the films become more opaque (Figure 11), no transmittance is seen in the visible region. Instead, a distinct peak is observed in the ultraviolet region of the transmittance spectra at 322 nm. This loss of transmittance in the visible region is a result of the light being absorbed by the films and is indicative of the film existing as a well-connected array of particles instead of clearly defined Ag NPs and is consistent with reports from the literature.[33–35] This connected array of particles in the thicker films is also corroborated by SEM images showing the same (Figure 10). These data demonstrate the success of these MOD inks in depositing conductive metal at low temperatures and opens wide avenues for developing electron circuits on flexible and renewable substrates.

Conclusion

This work has shown that Ag-amidinate MOD precursors are a versatile choice for metallic silver deposition: single-layer depositions produce highly transparent (>90% transmittance) Ag NP coatings which are reflective in the UV region, while layering can produce conductive Ag films (ρ = 0.916–1.83 × 10^{-6} Ωm), which have potential for use in electronic materials. Inks were produced from dissolving MOD precursors of the type: [Ag_2((ArN)$_2$C(H))$_2$] (Ar = 2,6-dimethylphenyl (**1**), 2,6-diethylphenyl (**2**) and 2,6-diisopropylphenyl (**3**)) in toluene, which were subsequently shown to fully convert to metallic Ag on glass substrates at temperatures considerably lower (200 °C) than the typical industrial standards for glass coatings (vapour deposition techniques utilize temperatures in excess of 400 °C). This indicates that there is potential for these inks to be used in conjunction with low glass transition temperature plastics or fabric. Thin films were characterized by numerous techniques including XRD, SEM, XPS and UV-Vis spectrometry, and ongoing efforts will continue to explore the deposition of these precursors on a wider variety of substrates.

Experimental

General procedures

All chemicals were obtained from Sigma-Aldrich and used without further purification. All syntheses with Ag(I) compounds were carried out in the absence of light. Nuclear Magnetic Resonance (NMR) data were collected using *Bruker Avance III* 400 MHz and *Avance III* 600 MHz instruments. Fourier transformation infra-red (FTIR) spectroscopy data were collected from 500–4000 cm^{-1} using an

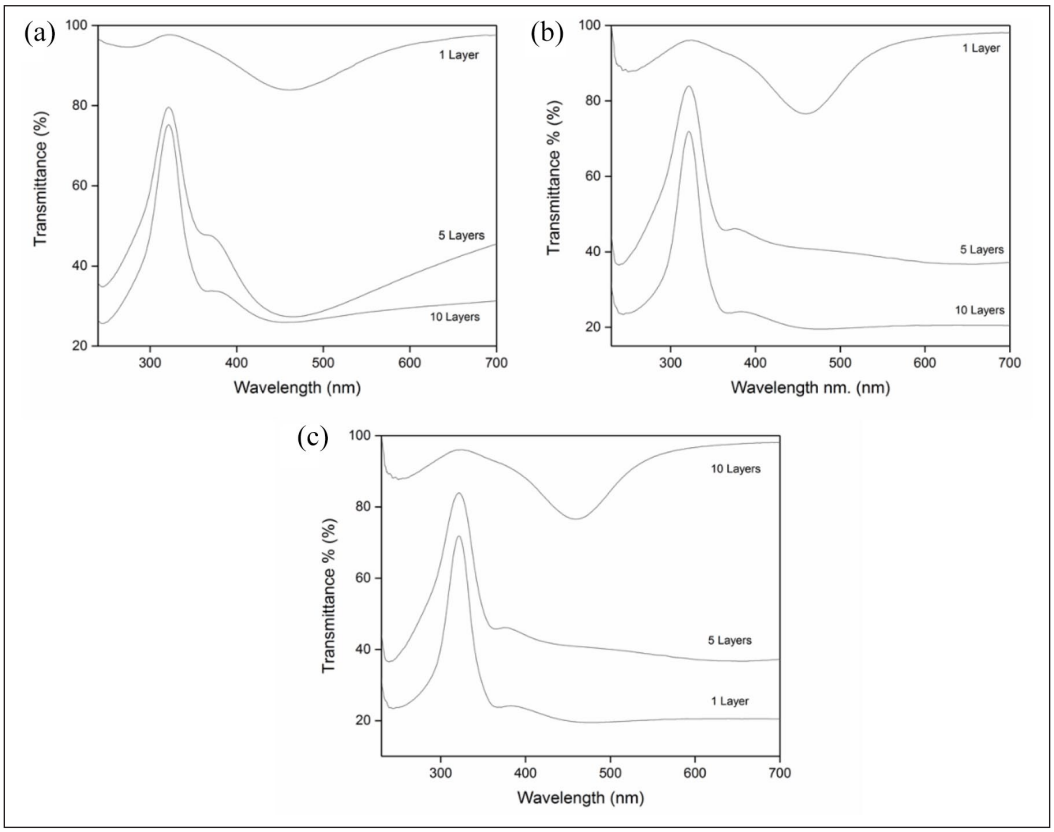

Figure 7. Transmittance spectra for single-layered, 5-layered and 10-layered films from (a) **I1**, (b) **I2** and (c) **I3**.

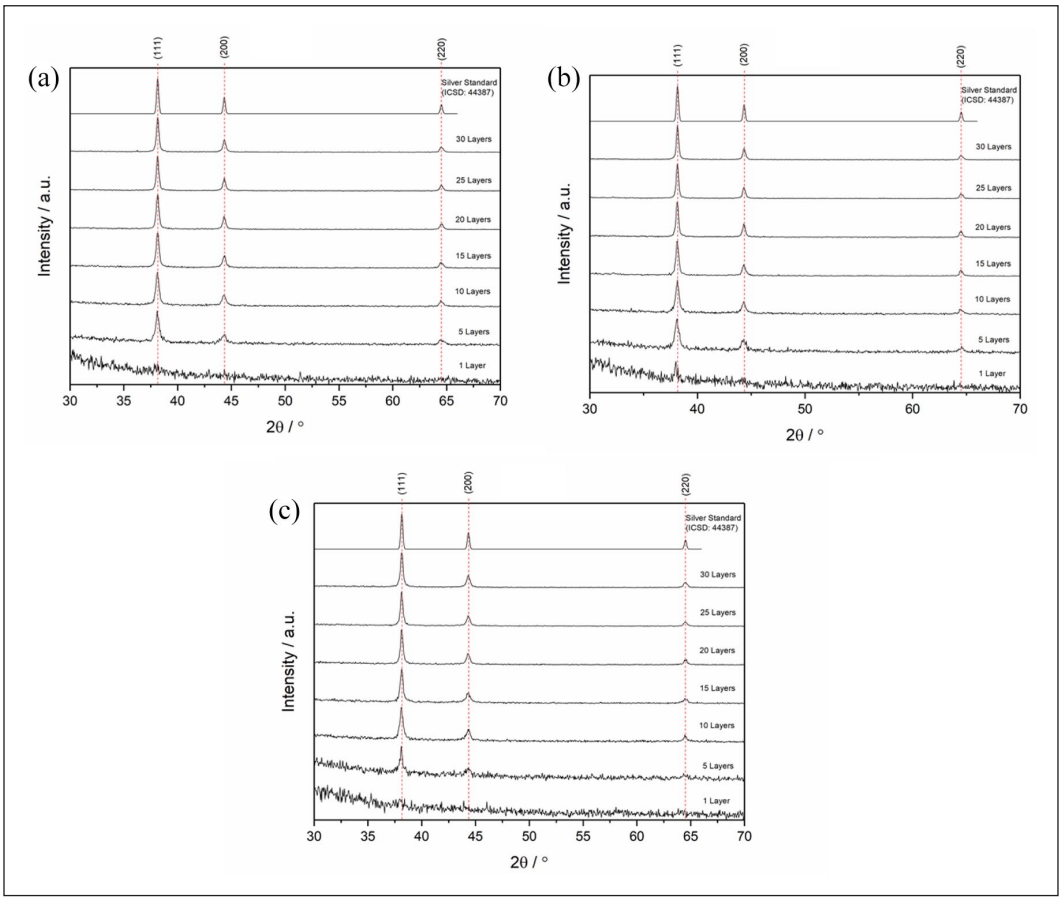

Figure 8. XRD plots for multi-layered Ag films deposited using (a) **I1** (b) **I2** and (c) **I3** and standard Ag data.

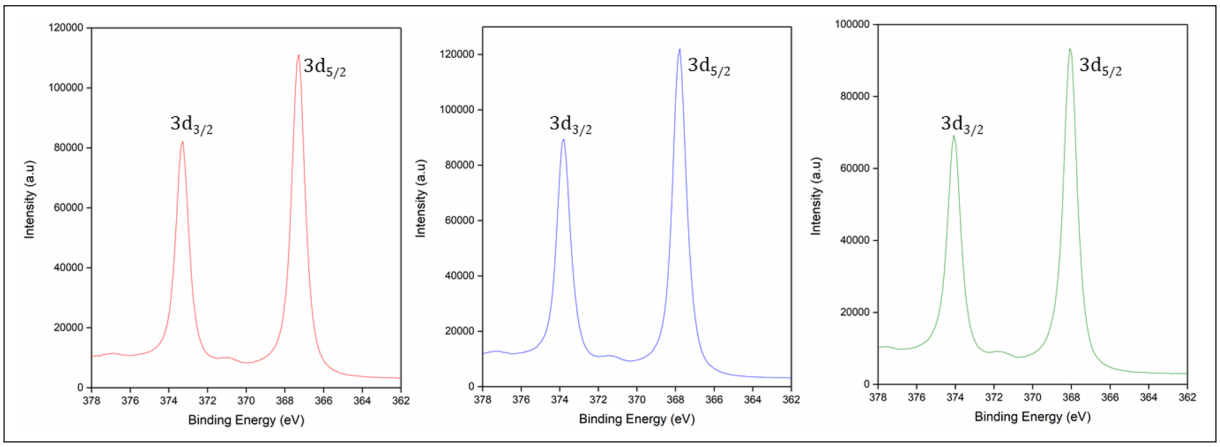

Figure 9. XPS data for 30-layered films deposited using **I1** (red), **I2** (blue) and **I3** (green).

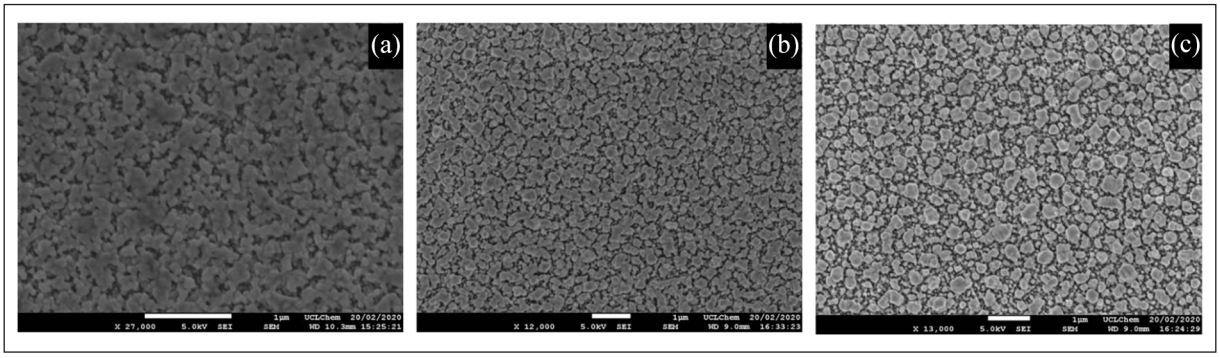

Figure 10. SEM images of 30-layered films obtained from (a) **I1** (b) **I2** and (c) **I3**.

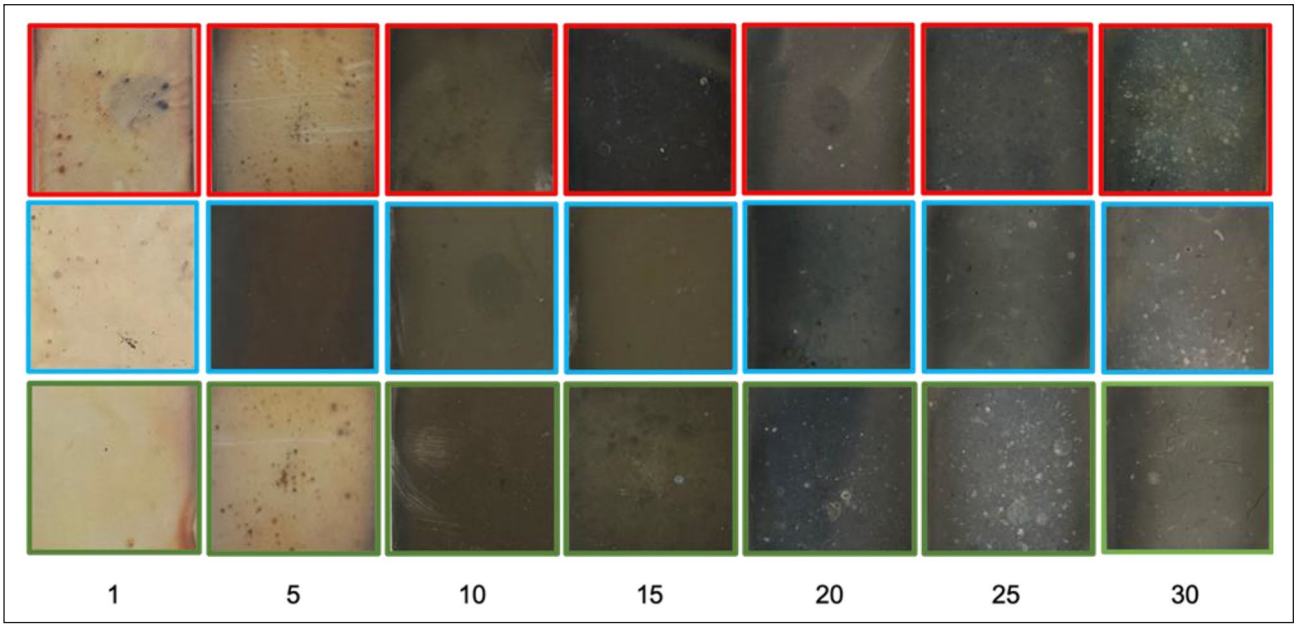

Figure 11. Images of films obtained from inks **I1** (red), **I2** (blue) and **I3** (green), spin-coated and sintered (number of layers indicated at the bottom).

ALPHA II FTIR spectrometer. TGA data were collected using a *Netzsch STA 449C Jupiter* instrument, with graphs being calibrated to 100%. Precursor samples were placed in an Al crucible and measurements were recorded from 20 to 400 °C. Single crystal X-ray diffraction (SCXRD) data were collected using a *SuperNova Atlas (Dual)* diffractometer using Cu K_α radiation at a wavelength of 1.54184 Å. A suitable crystal was chosen, mounted on a nylon loop and

kept at 150 K during data collection (CCDC 2126901). Electrospray ionization (ESI) and electron ionization (EI) mass spectra were attempted using *Waters LTC Premier XE ESI Q-TOF* mass spectrometer. Elemental analysis (EA) was collected by the Geosciences Department at the University of Edinburgh. Thin films were analysed as deposited.

L^{1}H: Triethyl orthoformate (4.16 mL, 25 mmol), 2,6-dimethylaniline (0.29 mL, 5 mmol) and glacial acetic acid (0.29 mL, 5 mmol) were combined together and heated at 160 °C for 16 h. The resulting solution was dried in vacuo to yield a solid which was dissolved in diethyl ether (130 mL) and neutralized with sodium carbonate (20 mL). The organic layer was extracted, dried with Na_2SO_4 and the solvent removed in vacuo. The resulting solid was recrystallized from acetone at −18 °C, yielding **L^{1}H** as colourless crystals (32%). ^{1}H NMR (400 MHz, $CDCl_3$): δ 7.13-6.88 (m, 6H, ArH), 5.55 (d, 1H, NH, $^3J_{H\text{-}H}$ = 12.2 Hz), 2.26 (d, 12H, CH_3, $^3J_{H\text{-}H}$ = 11.3 Hz).

L^{2}H: Triethyl orthoformate (3.33 mL, 20 mmol), 2,6-diethylaniline (6.59 mL, 40 mmol) and glacial acetic acid (0.23 mL, 4 mmol) were combined together and heated at 160 °C for 16 h. The resulting mixture was dried in vacuo to yield a solid which was dissolved in diethyl ether (130 mL) and neutralized with sodium carbonate (20 mL). The organic layer was extracted, dried with Na_2SO_4, and recrystallized at −18 °C, yielding **L^{2}H** as colourless crystals (65%). ^{1}H NMR (400 MHz, $CDCl_3$): δ 7.25-7.01 (m, 6H, ArH), 5.55 (d, 1H, NH, $^3J_{H\text{-}H}$ = 11.9 Hz), 2.83-2.49 (m, 8H, CH_2CH_3), 1.32-1.12 (m, 12H, CH_2CH_3).

L^{3}H: Triethyl orthoformate (3.24 mL, 19.5 mmol), 2,6-diisopropylaniline (7.9 mL, 39 mmol) and glacial acetic acid (0.21 mL, 3.9 mmol) were combined together and heated at 160 °C for 16 h. The resulting mixture was dried in vacuo to yield a yellow solid. The solid was dissolved in diethyl ether (150 mL) and neutralized with sodium carbonate (50 mL). The organic layer was extracted, dried with Na_2SO_4, and recrystallized at −18 °C, yielding **L^{3}H** as colourless crystals (43%). ^{1}H NMR (400 MHz, $CDCl_3$): δ 7.25-7.05 (m, 6H, ArH), 5.55 (d, 1H, NH, $^3J_{H\text{-}H}$ = 11.9 Hz), 3.42–3.13 (m, $CH(CH_3)_2$, 4H), 1.33 (d, 3H, $CH(CH_3)_2$, $^3J_{H\text{-}H}$ = 7.0 Hz), 1.25-1.07 (m, 21H, $CH(CH_3)_2$).

Synthesis of Ag(I) amidinate complexes

1. **L^{1}H** (1.5 g, 6 mmol) and triethylamine (2.439 mL, 18 mmol) were dissolved in dichloromethane (80 mL) and the reaction mixture was heated to 60 °C. Silver acetate (1.002 g, 6 mmol) was added to the mixture and the reaction left to heat for 20 min. The solution was hot filtered, cooled to room temperature and methanol was layered on top. The flask was inverted, and the solution was placed in the freezer for 3 days yielding off white crystals of **1** (87%). ^{1}H NMR (400 MHz, $CDCl_3$): δ 7.27 (t, 2H, $^3J_{H\text{-}Ag109}$ = 18.1 Hz, NC(H)N), 7.00 (d, 8H, ArH, $^3J_{H\text{-}H}$ = 7.7 Hz), 6.92–6.86 (m, 4H, ArH), 2.33 (s, 24H, CH_3). ^{13}C NMR ($CDCl_3$ 600 MHz): δ 19.7 (CH_3), 123.9 (Ar-C), 128.3 (Ar-C), 132.9 (Ar-C), 148.8 (Ar-C), 166.2 (NCN). IR ν_{max}/cm^{-1} 2949.2. EA/% ($C_{34}H_{38}Ag_2N_4$) calcd: C, 56.84; H, 5.33; N, 7.80; found: C, 57.48; H, 5.43; N, 7.76. Positive ESI MS: m/z 719 $[M]^+$.

2. **L^{2}H** (1.5 g, 4.8 mmol) and triethylamine (2.0 mL, 14.4 mmol) were dissolved in dichloromethane (10 mL) and the reaction mixture was heated to 50 °C. Silver acetate (0.802 g, 4.8 mmol) was added to this, and the reaction was left to heat for 20 min. The solution was hot filtered and then cooled to room temperature. Methanol was layered on top, the flask inverted and stored in the freezer to allow recrystallization. **2** was obtained as an off white crystalline solid (75%). ^{1}H NMR (600 MHz, $CDCl_3$): δ 7.24 (t, t, dd, 2H, $^3J_{H\text{-}Ag109}$ = 18.1 Hz, $^3J_{H\text{-}Ag107}$ = 15.7 Hz, $CH_{\mathbf{a}}$), 7.06-6.99 (m, 12H, ArH), 2.88-2.69 (m, 16H, CH_2CH_3), 1.27 (t, 24H, CH_2CH_3, $^3J_{H\text{-}H}$ = 7.5 Hz). ^{13}C NMR (600 MHz, $CDCl_3$): δ 165.8 (NCN), 147.6 (Ar-C), 124.4 (Ar-C), 25.1 (CH_2), 14.6 (CH_3). ν_{max}/cm^{-1} 2956.6, 2910 EA/% ($C_{42}H_{54}Ag_2N_4$) calcd: C, 60.74; H, 6.55; N, 6.75; found: C, 61.10; H, 6.57; N, 6.77.

3. **L^{3}H** (1.5 g, 4.1 mmol) and triethylamine (1.68 mL, 12.1 mmol) were dissolved in dichloromethane and the solution was heated to 50 °C. Silver acetate (0.69 g, 4.1 mmol) was added to the solution and the reaction mixture was allowed to heat for 20 min. The solution was then hot filtered, allowed to cool to room temperature and methanol was layered on top of the solution. The flask was inverted and stored in the freezer to allow recrystallization, yielding **3** as an off white solid (93%). ^{1}H NMR (600 MHz, $CDCl_3$): δ 7.23 (t, t, dd, 2H, $^3J_{H\text{-}Ag109}$ = 18.1 Hz, $^3J_{H\text{-}Ag107}$ = 15.7 Hz, $CH_{\mathbf{a}}$), 7.09-7.03 (m, 12H, ArH), 3.59 (hept, 8H, $CH(CH_3)_2$, $^3J_{H\text{-}H}$ = 6.9 Hz), 1.26 (d, 24H, $CH(CH_3)_2$, $^3J_{H\text{-}H}$ = 6.9 Hz), 1.18 (d, 24H, $CH(CH_3)_2$, $^3J_{H\text{-}H}$ = 6.9 Hz). ^{13}C NMR (151 MHz, $CDCl_3$): δ 166.0 (NCN), 145.8 (Ar-C), 143.5 (Ar-C), 123.4 (Ar-C), 27.8 (CH), 24.2 (CH_3), 23.6 (CH_3). ν_{max}/cm^{-1} 2961.5, 2861.5. EA/% ($C_{50}H_{70}Ag_2N_4$) calcd: C, 63.69; H, 7.48; N, 5.94; found: C, 63.70; H, 7.31; N, 5.96.

Ink preparation and thin film deposition

Physical measurements. Thin films were analysed as deposited. Thin-film XRD patterns were collected using a *Bruker AXS D8 discovery Lynx Eye* diffractometer. The X-rays were generated using a Cu Kα (40 kV, 40 mA), λ = 1.54056 Å. The incident beam angle was kept at 1° and data were collected between 2θ = 30° and 70° with a step size of 0.05° at 4.0 s/step. XPS measurements were collected using a *Thermo Scientific K-alpha photoelectron* spectrometer with a monochromatic Al K_α source. These data were calibrated against C(1s) adventitious carbon (284.6 eV) for charge correction using *CasaXPS* software. UV-Vis data were collected between 200 and 800 nm using *UV-2600 UV-Vis spectrophotometer*. SEM images were taken using a *JEOL 6301* filament scanning electron microscope. To minimize charging effects, these were taken at ranges from 3 to 5 kV. Before the images were taken, a fine layer of gold was

coated on the sample to stop charging on the surface. Energy-dispersive X-ray spectroscopy (EDS) was collected on a *Philips XL30SEM* instrument. Resistance was measured using a *Kewtech KT116 Digital Multimeter*.

Inks **I1**, **I2** and **I3** were prepared by dissolving **1**, **2** and **3**, respectively, in toluene at a concentration of 0.05 mol dm^{-3}. Thin films were deposited via spin coating using *Laurell Model WS-650 MZ-23NPPB* onto glass slides and sintered immediately after. 1000 r/min was found to be the optimal spin speed and all inks were deposited at 1000 r/min for 5 s. All inks were sintered on a hotplate heated to 200 °C for 15 min.

Declaration of conflicting interests

The author(s) declared no potential conflicts of interest with respect to the research, authorship and/or publication of this article.

Funding

The author(s) disclosed receipt of the following financial support for the research, authorship and/or publication of this article: The authors thank the EPSRC (EP/R513143/1) and the Ramsay Memorial Trust for funding.

ORCID iD

Caroline E Knapp https://orcid.org/0000-0003-4219-9313

Supplemental material

Supplemental material for this article is available online.

References

1. Silver – element information, properties and uses | Periodic table, https://www.rsc.org/periodic-table/element/47/silver (accessed 15 October 2021).
2. Bhide MA, Carmalt CJ and Knapp CE. *J Mater Chem* 2020; 8: 5501–5508.
3. Knapp CE, Chemin J-B, Douglas SP, et al. *Adv Mater Technol* 2018; 3: 1700326.
4. Misra N, Kumar V, Borde L, et al. *Sens Actuators B Chem* 2013; 178: 371–378.
5. McFarland AD and Van Duyne RP. *Nano Letters* 2003; 3: 1057–1062.
6. Pozo D. *Silver nanoparticles*. Norderstedt: BoD – Books on Demand, 2010.
7. Tinker HR, Bhide MA, Magliocca E, et al. *J Mater Sci* 2021; 56: 6966–6976.
8. Knapp CE, Metcalf EA, Mrig S, et al. *ChemistryOpen* 2018; 7: 850–857.
9. Bhide MA, Manzi JA, Knapp CE, et al. *Molecules* 2021; 26: 3165.
10. Douglas SP and Knapp CE. *ACS Appl Mater Interfaces* 2020; 12: 26193–26199.
11. Walker SB and Lewis JA. *J Am Chem Soc* 2012; 134: 1419–1421.
12. Vaseem M, McKerricher G and Shamim A. *ACS Appl Mater Interfaces* 2016; 8: 177–186.
13. Bhat KS, Ahmad R, Wang Y, et al. *J Mater Chem C* 2016; 4: 8522–8527.
14. Bhide MA, Mears KL, Carmalt CJ, et al. *Chem Sci* 2021; 12: 8822–8831.
15. Knapp CE and Carmalt CJ. *Chem Soc Rev* 2016; 45: 1036–1064.
16. Douglas SP, Mrig S and Knapp CE. *Chem: Eur J* 2021; 27: 8062–8081.
17. Manzi JA, Knapp CE, Parkin IP, et al. *Eur J Inorg Chem* 2015; 22: 3658–3665.
18. Knapp CE, Marchand P, Dyer C, et al. *New J Chem* 2015; 39: 6585–6592.
19. Archibald SJ, Alcock NW, Busch DH, et al. *Inorg Chem* 1999; 38: 5571–5578.
20. Whitehorne TJJ, Coyle JP, Mahmood A, et al. *Eur J Inorg Chem* 2011; 2011: 3240–3247.
21. Cervantes Reyes A, Rominger F, Rudolph M, et al. *Chemistry* 2019; 25: 11745–11757.
22. Peddarao T, Baishya A, Barman MK, et al. *New J Chem* 2016; 40: 7627–7636.
23. Lane AC, Vollmer MV, Laber CH, et al. *Inorg Chem* 2014; 53: 11357–11366.
24. Tate BK, Wyss CM, Bacsa J, et al. *Chem Sci* 2013; 4: 3068–3074.
25. Bhui DK, Bar H, Sarkar P, et al. *J Mol Liq* 2009; 145: 33–37.
26. Mohamedkhair AK, Drmosh QA and Yamani ZH. *Front Mater* 2019; 6: 188.
27. Homola J. *Anal Bioanal Chem* 2003; 377: 528–539.
28. Hoflund GB, Weaver JF and Epling WS. *Surf Sci Spectra* 1994; 3: 151–156.
29. Liu Y, Jordan RG and Qiu SL. *Phys Rev B* 1994; 49: 4478–4484.
30. Seah MP, Gilmore IS and Beamson G. *Surf Interface Anal* 1998; 26: 642–649.
31. Fuggle JC, Källne E, Watson LM, et al. *Phys Rev B* 1977; 16: 750–761.
32. Choi Y, Seong K and Piao Y. *Adv Mater Interfaces* 2019; 6: 1901002.
33. Yamaguchi T, Yoshida S and Kinbara A. *Thin Solid Films* 1973; 18: 63–70.
34. Doremus RH. *J Colloid Interf Sci* 1968; 27: 412–418.
35. Yamaguchi T, Yoshida S and Kinbara A. *Thin Solid Films* 1974; 21: 173–187.